ЖЭТФ, 1999, том 115, вып. 6, стр. 2170–2189

LATTICE VIBRATIONS OF α'-NaV_2O_5

M. N. Popova, A. B. Sushkov, S. A. Golubchik, B. N. Mavrin, V. N. Denisov*

Institute of Spectroscopy, Russian Academy of Sciences
142092, Troitsk, Moscow Region, Russia

B. Z. Malkin, A. I. Iskhakova

Kazan State University
420008, Kazan, Russia

M. Isobe, Y. Ueda

Institute for Solid State Physics, University of Tokyo
7-22-1 Roppongi, Minato-ku, Tokyo 106, Japan

Submitted 10 Semtember 1998

We have measured far infrared reflectance and transmittance spectra as well as Raman scattering spectra of α'-NaV_2O_5 single crystals for all the principal polarizations. The temperature range above the phase transition temperature $T_c = 35$ K was investigated, mainly. On the basis of this experimental study and of the lattice dynamics calculations we conclude that the symmetry of NaV_2O_5 in the high-temperature phase is described by the centrosymmetric D_{2h}^{13} space group. This conclusion leads to important physical consequences concerning the interpretation of one-dimensional magnetic properties of NaV_2O_5 and of the phase transition at 35 K considered earlier to be an ordinary spin-Peierls transition. The assignment of the observed phonons is given. Values of dielectric constants are obtained from the infrared data. Asymmetric shapes of several infrared lines and higher-order infrared vibrational spectra are discussed. The crystal field energy levels of the $3d$ electron localized at the V^{4+} site have been calculated in the framework of the exchange charge model using the values of effective charges obtained from the lattice dynamics calculations. According to the results of these calculations, the broad optical bands observed earlier in the vinicity of 1 eV can be interpreted as phonon assisted d–d transitions.

1. INTRODUCTION

The vanadate α'-NaV_2O_5 has attracted considerable interest recently as the second inorganic compound undergoing the spin-Peierls transition (at the highest known temperature for the spin-Peierls compounds, $T_c = 35$ K [1]). The spin-Peierls transition is expected to occur within a system of linear spin-1/2 Heisenberg antiferromagnetic chains coupled to a three-dimensional phonon field. As a result of such a coupling, magnetic atoms of the chain dimerize and a spin gap opens [2]. One-dimensional magnetic properties of NaV_2O_5 above 35 K follow from magnetic susceptibility [1], ESR [3] and angle-resolved photoemission [4] measurements.

Below 35 K the lattice dimerizes, as observed by X-ray [5] and Raman [6, 7] scattering, infrared transmission [8] and reflection [9] measurements, while the magnetic susceptibility

*E-mail: popova@isan.troitsk.ru

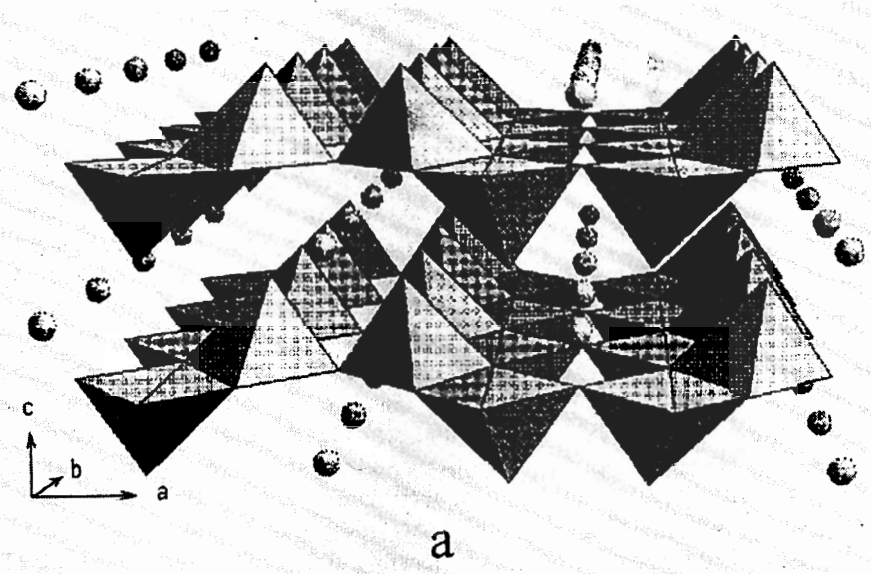

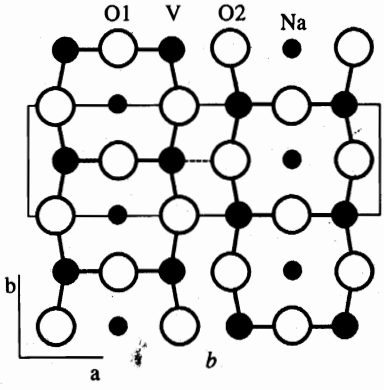

Fig. 1. Structure of NaV_2O_5. a) Stereometric projection. Oxygen and vanadium atoms are at the corners of and inside the pyramids, respectively. Sodium atoms are represented by balls. b) *ab* projection. Apical oxygen O3 atoms (situated above or below the corresponding V atoms) are not shown. A dashed line indicates the longest V–O2 bond (0.199 nm). *ab*-projection of the crystal unit cell is shown by a thin solid line

decreases isotropically, thus showing a spin gap formation [6]. The size of the gap $\Delta = 10$ meV follows from inelastic neutron scattering study of NaV_2O_5 single crystals [5, 10].

The structure of NaV_2O_5 contains double chains of edge-sharing distorted VO_5 pyramids running along the orthorhombic *b*-axis (Fig. 1). These double chains are linked via common corners of the pyramids to form the *ab*-layers. Na atoms lie between the layers [1, 11]. The structure of NaV_2O_5 looks like the structure of V_2O_5 [12] intercalated with sodium. In an early X-ray room temperature investigation on polycrystalline samples of NaV_2O_5, Carpy and Galy [11] suggested the noncentrosymmetric space group C_{2v}^7-$P2_1mn$ with two nonequivalent vanadium positions in the unit cell. The picture of magnetic chains of $V^{4+}O_5$ ($S = 1/2$) pyramids isolated by nonmagnetic chains of $V^{5+}O_5$ ($S = 0$) pyramids proposed to account for

one-dimensional magnetic properties of this mixed valence ($V^{4.5+}$) compound is compatible with this space group [1].

However, the recent redetermination of the structure by single crystal X-ray diffraction at room temperature was in favor of the centrosymmetric D_{2h}^{13}-$Pmmn$ group with only one vanadium position in the structure [13, 14]. Though the topology of the structure remains essentially the same as in the previously proposed noncentrosymmetric space group [11], the possibility for charge ordering is, however, lost in the new higher symmetry group. Smolinski at al. [13] and Horsch and Mack [15] suggested a quarter-filled ladder model for NaV_2O_5, with the spins carried by V–O–V molecular orbitals on the rungs of the ladder. They argued that the exchange interaction along the ladder is much greater than that between the neighboring ladders which would explain the one-dimensional magnetic properties of the high temperature phase of NaV_2O_5. The transition at 35 K was supposed to be an ordinary spin-Peierls transition. Quite recent ^{51}V-NMR experiment on a single-crystalline sample of NaV_2O_5 also revealed only one vanadium position in the high-temperature phase but pointed unambiguously to the existence of two different vanadium sites occupied by V^{4+} and V^{5+} at liquid-helium temperatures [16]. Thus, the transition at 35 K is connected with a structure and charge ordering processes. Very recently, Seo and Fukuyama [17] and Mostovoy and Khomskii [18] proposed a zigzag scheme of V^{4+}–V^{5+} ordering. Seo and Fukuyama argued that, as a result, two-dimensional lattice of antiferromagnetic dimers is formed [17], while Mostovoy and Khomskii gave reasons in support of a system of alternating chains [18]. Thalmeier and Fulde [19] have presented some theoretical reasons for the primary charge ordering which provides neighboring linear V^{4+} and V^{5+} chains with a subsequent spin-Peierls transition. Two close transitions near 35 K in NaV_2O_5 were detected by Köppen et al. via thermal expansion measurements [20].

In view of these recent works, the symmetry problem of the high-temperature phase seems to be a matter of great urgency. Raman and infrared measurements could give additional information to clarify whether the space group is centrosymmetric or not, because of totally different selection rules in these two cases. We reanalyzed our earlier infrared and Raman spectra of NaV_2O_5 [21] and found that they are in a better agreement with the centrosymmetric D_{2h}^{13} space group than with the noncentrosymmetric C_{2v}^{7}. However, in our work [21] we did not measure infrared spectra in the $\mathbf{E}||\mathbf{c}$ polarization. Also, the signal-to-noise ratio of Raman spectra was rather low. In the present work, we reinvestigate vibrational spectra of the high-temperature phase of NaV_2O_5 using different single crystals, including extraordinary big ones. We present far-infrared reflectivity as well as Raman-scattering spectra for all principal polarizations. In addition, transmittance spectra were studied. We show that our results are in a much better agreement with the centrosymmetric D_{2h}^{13} group than with the noncentrosymmetric C_{2v}^{7}. The assignment of vibrational modes is given. It is based on a comparison with results of the previously studied of V_2O_5 [22] and on lattice dynamics calculations of this work performed in the framework of the rigid-ion model.

2. EXPERIMENTAL

Single crystals of stoichiometric α'-NaV_2O_5 used in this study were grown by a melt growth method using $NaVO_3$ as a flux [23]. Samples from different batches were used. One sample was $1.3 \times 8 \times 1$ mm, another one was $3 \times 17.3 \times 1.6$ mm along a-, b-, and c-axes, respectively. For transmission measurements we have prepared four thin samples cleaved perpendicular to the c-axis. Their thicknesses were 110 ± 1, 45 ± 5, 14 ± 1.5 and 6 ± 1 μm. The samples

were checked with X-ray diffraction, magnetization, and ESR measurements. They exhibited a sharp transition at about 35 K.

Reflection and transmission measurements were performed with a BOMEM DA3.002 Fourier transform spectrometer at nearly normal incidence of polarized infrared radiation. The following geometries of the experiment were used: 1) **k**||**c**, **E**||**a** and **E**||**b**; 2) **k**||**a**, **E**||**c** and **E**||**b**. Room-temperature reflectance and transmittance spectra were measured in a spectral range 30–5000 cm^{-1} with a resolution 0.5–2.0 cm^{-1}. Using both reflectance and transmittance spectra, the absorption coefficient α was calculated. Low-temperature (down to 6 K) transmittance spectra were measured with a He vapor cryostat in the spectral range 30–1000 cm^{-1} with a resolution 0.05–1.0 cm^{-1}.

Raman spectra were excited at room temperature by the 514-nm and 488-nm lines of an Ar-ion laser in backscattering geometries, dispersed by a home-made triple spectrograph, and recorded using a multichannel system consisting of an image intensifier tube with a multichannel plate and a vidicon.

3. RESULTS

3.1. Factor-group analysis

There are two formula units and, hence, 16 atoms in the NaV_2O_5 orthorhombic unit cell with lattice constants $a = 1.1316$ nm, $b = 0.3611$ nm, $c = 0.4797$ nm [11, 13, 14]. Below, we present the results of factor-group analysis for both centrosymmetric D_{2h}^{13} [13, 14] and noncentrosymmetric C_{2v}^{7} [11] space groups.

a. *Space group* D_{2h}^{13}-*Pmmn*. The notation *Pmmn* refers to the standard axis setting, such that **x**||**a**, **y**||**b**, **z**||**c**. It follows from X-ray diffraction data [13, 14] that Na atoms occupy $2b$ positions (the corresponding fractional atomic coordinates are defined by the basis vectors $\mathbf{r}_1(\mathrm{Na}) = -\mathbf{r}_2(\mathrm{Na}) = (1/4, -1/4, z_1)$, $z_1 = 0.8592$, and oxygen O1 atoms occupy $2a$ positions ($\mathbf{r}_1(\mathrm{O1}) = -\mathbf{r}_2(\mathrm{O1}) = (1/4, 1/4, z_2)$, $z_2 = 0.5195$), both these positions having C_{2v}^{z} local symmetry. V, O2 and O3 atoms reside in different $4f$ positions ($\mathbf{r}_1(\mathrm{A}) = -\mathbf{r}_3(\mathrm{A}) = (x_\mathrm{A}, 1/4, z_\mathrm{A})$, $\mathbf{r}_2(\mathrm{A}) = -\mathbf{r}_4(\mathrm{A}) = (1/2 - x_\mathrm{A}, 1/4, z_\mathrm{A})$; A = V, O2, O3; $x_\mathrm{V} = 0.40212$, $z_\mathrm{V} = 0.39219$, $x_{\mathrm{O2}} = 0.57302$, $z_{\mathrm{O2}} = 0.48769$, $x_{\mathrm{O3}} = 0.38548$, $z_{\mathrm{O3}} = 0.05803$) with the local symmetry C_s^{xz}. These positions yield the following irreducible representations [24, 25]:

$$C_{2v}^{z} : \Gamma = A_g + B_{2g} + B_{3g} + B_{1u} + B_{2u} + B_{3u},$$

$$C_s^{xz} : \Gamma = 2A_g + B_{1g} + 2B_{2g} + B_{3g} + A_u + 2B_{1u} + B_{2u} + 2B_{3u}.$$

Multiplying the representations given above by the number of different positions of the appropriate symmetry, summarizing them, and subtracting acoustic modes ($B_{1u} + B_{2u} + B_{3u}$), we obtain the following NaV_2O_5 optical vibrational modes:

$$\Gamma^{vib}_{NaV_2O_5}(Pmmn) = 8A_g(aa, bb, cc) + 3B_{1g}(ab) + 8B_{2g}(ac) + 5B_{3g}(bc) + 3A_u + \\ + 7B_{1u}(\mathbf{E}||\mathbf{c}) + 4B_{2u}(\mathbf{E}||\mathbf{b}) + 7B_{3u}(\mathbf{E}||\mathbf{a}). \qquad (1)$$

There are 45 vibrational modes in total. A_u modes being silent, 24 Raman (A_g, B_{1g}, B_{2g}, B_{3g}) and 18 infrared (B_{1u}, B_{2u}, B_{3u}) active modes are expected to be found in the spectra of NaV_2O_5, provided the crystal space group is D_{2h}^{13}.

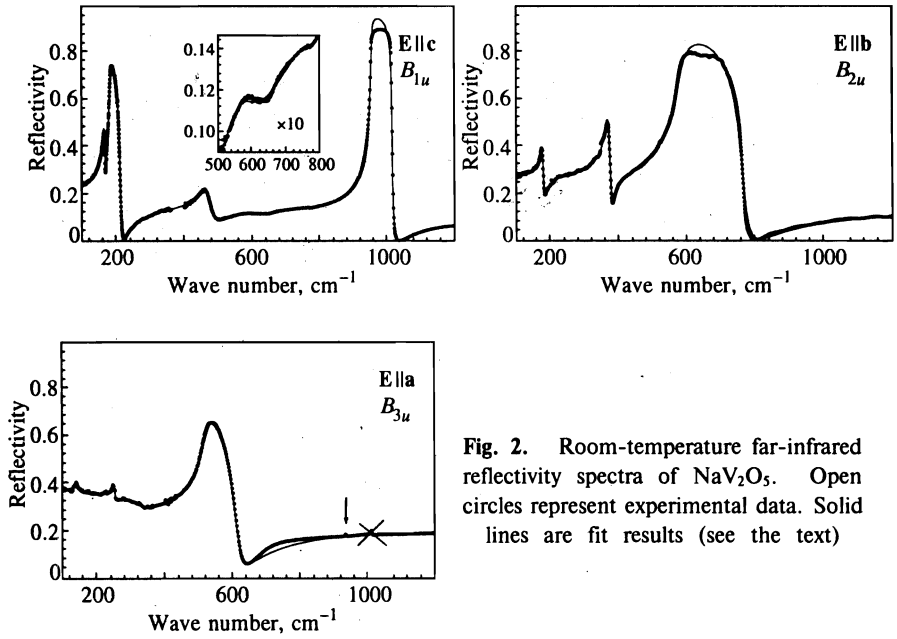

Fig. 2. Room-temperature far-infrared reflectivity spectra of NaV_2O_5. Open circles represent experimental data. Solid lines are fit results (see the text)

b. *Space group* C_{2v}^7-$P2_1mn$. In their original work [11], Carpy and Galy adopted the axis setting for the $P2_1mn$ space group. Below, we use the standard setting for the $Pmn2_1$ space group: $x||b$, $y||c$, $z||a$. There are two nonequivalent V positions, five nonequivalent O positions and one Na position in this group, all of them being $2a$ positions with C_s^{yz} local symmetry. In the same way as in the previous case, using tables [25] and subtracting acoustic modes ($A_1 + B_2 + B_1$), we find the following vibrational modes:

$$\Gamma_{NaV_2O_5}^{vib}(Pmn2_1) = 15A_1(aa, bb, cc; \mathbf{E}||\mathbf{a}) + 8A_2(bc) + 7B_1(ab; \mathbf{E}||\mathbf{b}) + 15B_2(ac; \mathbf{E}||\mathbf{c}). \quad (2)$$

There are 45 optical modes again. But in the case of this noncentrosymmetric space group all of them are Raman active, 37 of them are also infrared active.

3.2. Infrared spectra

Figure 2 shows the room temperature far-infrared reflectivity spectra of NaV_2O_5 for different polarizations of the incident light. Experimental data are presented by open circles. Measured spectra were least-squares fitted by the spectra computed according to the expression

$$\mathscr{R} = \left|\frac{\sqrt{\varepsilon} - 1}{\sqrt{\varepsilon} + 1}\right|^2. \quad (3)$$

The classical dispersion formula for N independent damped oscillators was used:

$$\varepsilon = \varepsilon_\infty + \sum_{i=1}^{N} \frac{4\pi f_i \omega_i^2}{\omega_i^2 - \omega^2 - i\gamma_i\omega}. \quad (4)$$

For **E||b** and **E||a** polarizations the number of oscillators and initial values of parameters were taken from the transmittance spectra ([21] and the present work). The anomaly crossed out

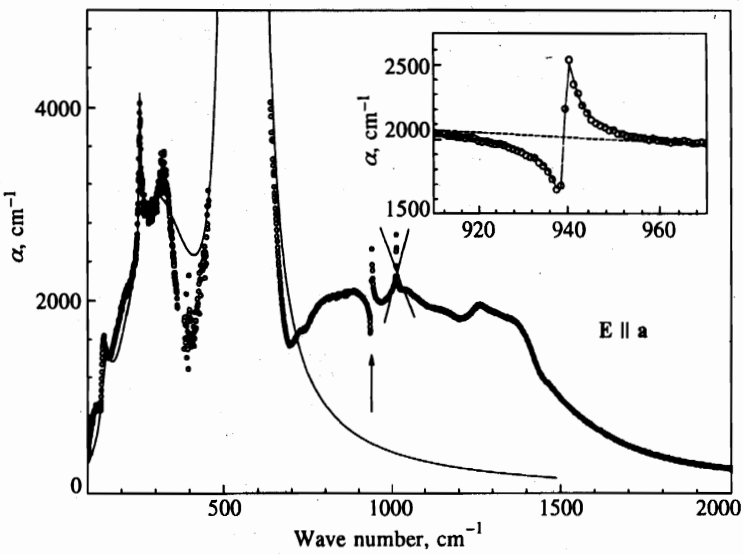

Fig. 3. Absorption coefficient α in the region of low-frequency absorption bands at room temperature. The arrow indicates a Fano-type resonance, shown separately in the inset. Open circles represent experimental data. Solid line in the main figure was calculated using the parameters obtained by fitting the reflectance spectrum. Solid line in the inset is a result of fitting the expression (5) with $\alpha_B(\omega)$, shown as a dashed line

in Figs. 2 and 3 at 1014 cm^{-1} in **E||a** polarization and also observed in **E||b** polarization for some samples depends on a particular sample, and is evidently not an intrinsic property of NaV_2O_5. It was not taken into account in the fitting procedure. In addition to weakly damped phonon oscillators, an overdamped oscillator centered at about 300 cm^{-1} (ω_i = 291 cm^{-1}, γ_i = 260 cm^{-1}, f_i = 0.38) was introduced in **E||a** polarization to account for a low-frequency part of a broad absorption band of a complex two-humped shape found in our previous study [21] (see also Fig. 3). We failed to model the high-frequency hump of this band centered at about 1000 cm^{-1} with a similar oscillator, and did not try to use a more complicated model. This results in only a fair fit to the hight-frequency part of the reflectance spectrum. In **E||a** polarization the phonon at about 150 cm^{-1} could not be fitted well. This line is strongly asymmetric in transmittance spectra, obviously due to interaction with the underlying broad band.

The small bump in reflection at 939 cm^{-1} shown by the arrow in Fig 2 corresponds to the Fano-type resonance [26] well seen in the absorbance spectrum (Fig. 3). One more such resonance becomes visible below 200 K at about 91 cm^{-1} (see Fig. 4 and also Ref. [8]). We fitted the absorption coefficient in the vicinity of these two strongly asymmetric lines by the expression [26]:

$$\alpha(\omega) = \alpha_B(\omega) + \alpha_0 \frac{q^2 + 2\xi q - 1}{1 + \xi^2}, \qquad (5)$$

where $\xi = (\omega - \omega_\tau)/\gamma$, $\alpha_B(\omega)$ is a slowly varying broad band absorption (it is shown as a dashed line in the vicinity of the 939-cm^{-1} sharp resonance in Fig. 3), and α_0, ω_τ, γ and q

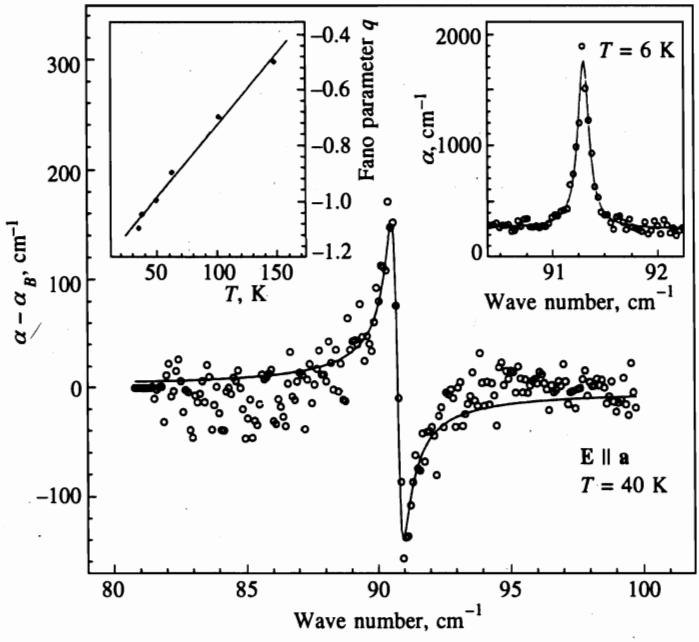

Fig. 4. Fano resonance near 91 cm^{-1} at 40 K (open circles) and its fit using Eq. (5) with parameters $\omega_\tau = 90.7$ cm^{-1}, $\gamma = 0.2$ cm^{-1}, $q = -1.0$, $\alpha_B(\omega_2) = 270$ cm^{-1}, and $\alpha_0/\alpha_B = 0.3$ (solid line). The temperature dependence of the Fano parameter q is given in the left inset. The right inset presents the absorbance spectrum in the vicinity of 91 cm^{-1} at 6 K with resolution 0.05 cm^{-1} (open circles), and Lorenzian fit with FWHM = 0.10 cm^{-1}

are variable parameters. Such an expression describes various physical situations for a sharp transitions overlapped by a broad continuum. The line shape of the sharp transition is altered by interference with a continuum, and depends heavily on the strength of the interaction between discrete and continuum states. The parameter q being inversely proportional to the matrix element of an interaction, the case $|q| = \infty$ corresponds to zero interaction and results in a normal Lorenzian resonance, $|q| = 1$ yields a dispersion-like curve, while $|q| = 0$ gives an inverted Lorenzian (antiresonance). The ratio α_0/α_B shows what fraction of the continuum states interacts with a sharp excited state. The results of fitting are displayed in the inset of Fig. 3 and in Fig. 4. A similar fit should be performed for the resonance at about 150 cm^{-1} but we failed to construct $\alpha_B(\omega)$ in this case. The fit parameters obtained are listed in Table 1; ω_{TO} and γ_{TO} denote ω_i and γ_i of Eq. (4) or ω_τ and γ of Eq. (5). LO frequencies and damping constants were calculated as complex roots of the equation $\varepsilon(\omega) = 0$.

The left inset of Fig. 4 presents the temperature dependence of the Fano parameter q for the spectral line near 91 cm^{-1} at temperatures higher than $T_c = 35$ K. It should be mentioned that below 35 K, the shape of this line changes to an ordinary Lorenzian (see the right inset of Fig. 4 and also [8]). Simultaneously, continuum absorption diminishes markedly in this spectral region while it is essentially unchanged at the maximum of the low-frequency hump at 320 cm^{-1}.

With decreasing the temperature, besides the asymmetric resonance at 91 cm^{-1} in **E||a** transmittance, two lines at 215 and 225 cm^{-1} appear in **E||b** transmittance spectra as well [8, 21].

Table 1

Infrared active vibrational modes (cm^{-1}) and dielectric constants of NaV_2O_5

Polarization, mode symmetry	Observed													Calculated ($Pmmn$)	
	Transmission						Reflection								
	T = 40 K		T = 300 K				T = 300 K								
	ω_{TO}	γ_{TO}	ω_{TO}	γ_{TO}	$\varepsilon^a_{\omega_1}$	$\varepsilon^a_{\omega_2}$	ω_{TO}	γ_{TO}	ω_{LO}	γ_{LO}	$10^3 f$	ε_∞	ε_0	ω_{TO}	ω_{LO}
E||c						7.5 ±0.2	162	5.2	165	5.7	45	3.9	7.7	216	219
$B_{1u}(Pmmn)$							179	8.4	212	8.3	130			232	256
or							–							298	298
$B_2(Pmn2_1)$							468	38.0	483	38.0	23			430	430
							591	119.9	597	119.0	6.8			589	690
							760	59.4	762	59.3	1.6			691	716
							955	2.5	1017	3.0	39			961	1036
E||b	178	4	175	12	5.2 ±0.2	10.2 ±0.2	175	8.3	180	8.4	39	4.9	9.5	141	173
$B_{2u}(Pmmn)$	225	1	–											240	266
or	371		367	16			365	12.8	378	13.3	60			388	483
$B_1(Pmn2_1)$	594	13	582				584	29.5	769	29.0	271			578	747
E||a	91[c]		–		9.6 ±0.3	15.0 ±0.6						7.7	15.8	111	126
$B_{3u}(Pmmn)$	140[b]		145[b]				153	33.0	155	34.1	46			130	177
or	254		251				251	7.3	252	8.2	9			227	276
$A_1(Pmn2_1)$	–	–					–							493	534
	531	18	526	53			525	39.5	622	52.4	208			538	653
	–						–							742	808
			939[d]											955	957

[a] ω_1 = 3200 cm^{-1}, ω_2 = 40 cm^{-1}.
[b] Asymmetric line.
[c] Fano-type resonance: ω_r = 90.7 cm^{-1}, γ = 0.2 cm^{-1}, q = −1.0, α_0/α_B = 0.3.
[d] Fano-type resonance: ω_r = 939 cm^{-1}, γ = 1.0 cm^{-1}, q = 1.1, α_0/α_B = 0.2.

We have studied the resonances at 91 and 939 cm^{-1} (**E||a**); 215 and 225 cm^{-1} (**E||b**) for the samples of different thicknesses, and found that while the intensities of 91-, 939- and 225-cm^{-1} lines are proportional to the sample thickness d (that is, α = const), the intensity of the 215-cm^{-1} line is essentially independent of the thickness ($\alpha d \simeq$ const). Consequently, while the frequencies 91 and 939 cm^{-1} (**E||a**) and 225 cm^{-1} (**E||b**) correspond to intrinsic resonances, ω = 215 cm^{-1} must refer to a surface excitation. All the observed infrared phonon frequencies together with the calculated ones are displayed in Table 1.

NaV_2O_5 crystals are well transparent in the frequency region between 2500 and 4500 cm^{-1}

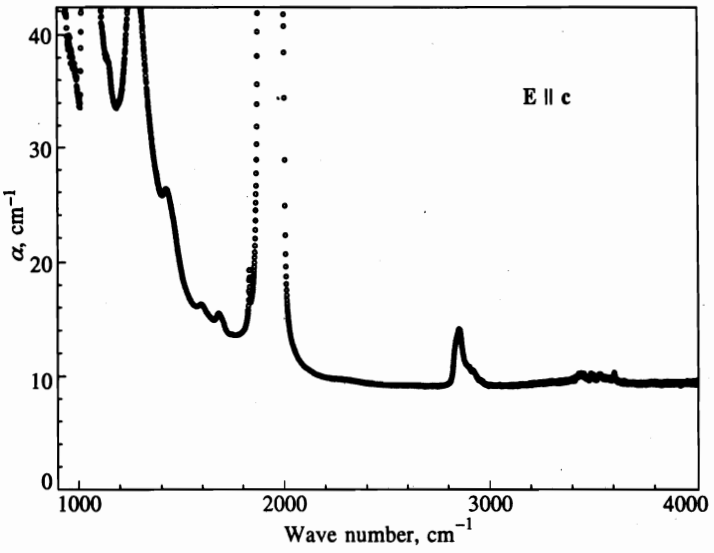

Fig. 5. Absorbance spectrum of NaV_2O_5 in the region of multiphonon bands at room temperature

and below 100 cm^{-1}. In these regions, an interference pattern was observed in **E||a** and **E||b** transmittance spectra of the samples of good quality. We also managed to observe the interference pattern below 100 cm^{-1} in **E||c** transmittance of 1.3-mm thick sample. By measuring the distances Δ between the interference maxima, we found the refractive indexes n according to the relation

$$\Delta = \frac{1}{2dn}. \tag{6}$$

Appropriate values of $\varepsilon = n^2$ are listed in Table 1.

We also looked for the higher-order vibrational spectra by measuring the transmittance of thick (d = 0.4–3.0 mm) samples in the frequency range 1000–4000 cm^{-1}. While no pronounced features were found in **E||a** and **E||b** polarizations, sharp resonances were observed in **E||c** (**k||a**) polarization at 1930, 2858 and possibly 1072 and 1270 cm^{-1}, the latter two lines being somewhat masked by the edge of a strong phonon at 955 cm^{-1} (Fig. 5).

3.3. Raman spectra

Polarized room-temperature Raman spectra of NaV_2O_5 in the spectral range 80–1000 cm^{-1} are shown in Fig. 6. One can see immediately that the three diagonal components aa, bb, cc of the Raman scattering tensor differ markedly one from another, which points to considerable anisotropy of the structure. The most intense spectra were observed in the A_g geometry $a(cc)\bar{a}$. The intensity of the lines marked by asterisks in B_{ig} ($i = 1, 2, 3$) spectra depended strongly on slight variations in the sample orientation. Probably, these lines are due to a leakage of strong lines from A_g geometries. We failed to assign for certain a weak feature near 100 cm^{-1} in the $b(ac)\bar{b}$ spectrum overlapped by a strong unshifted line that is present in this geometry. It might-possibly come from the leakage of a very strong line 90 cm^{-1} from the (cc) polarization.

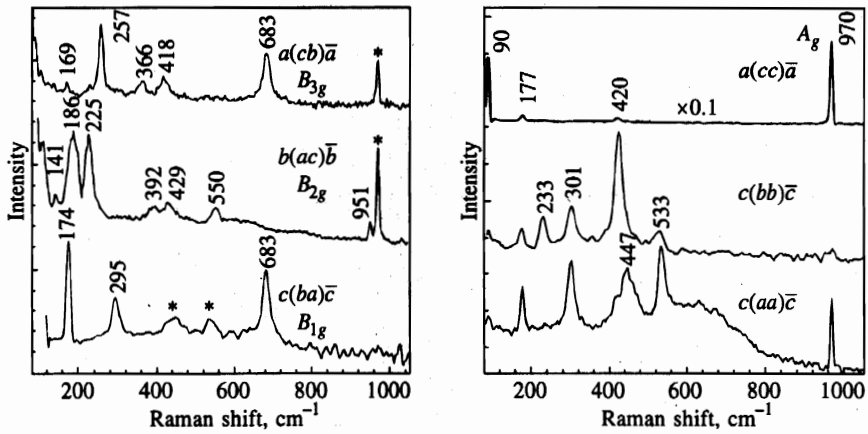

Fig. 6. Room-temperature Raman spectra of NaV_2O_5. Asterisks label A_g lines seen in B_{ig} $(i = 1, 2, 3)$ spectra

Table 2

Room-temperature Raman frequencies (cm^{-1}) for NaV_2O_5

aa, bb, cc $A_g(Pmmn)$ or $A_1(Pmn2_1)$		ab $B_{1g}(Pmmn)$ or $B_1(Pmn2_1)$		ac $B_{2g}(Pmmn)$ or $B_2(Pmn2_1)$		bc $B_{3g}(Pmmn)$ or $A_2(Pmn2_1)$	
Observed	Calc. $(Pmmn)$	Observed	Calc. $(Pmmn)$	Observed	Calc. $(Pmmn)$	Observed	Calc. $(Pmmn)$
90 (cc, aa)	91	174	191	141	129	169	149
177 (aa, bb, cc)	226	295	288	186	193	257	239
233 (bb)	319	683	679	225	296	366	262
301 (aa, bb)	362			392	332	418	396
420 (bb, cc)	439			429	410	683	685
447 (aa)	518			550	619		
533 (aa, bb)	626			–	798		
970 (cc, aa)	964			951	961		

Frequencies of the observed Raman modes together with the calculated ones are collected in Table 2.

As we have already reported [21], besides relatively narrow lines, a broad band with a maximum near 600 cm^{-1} is observed in the $c(aa)\bar{c}$ spectrum (see Fig. 6). Since this band appears under both 514.5-nm and 488-nm excitation, we conclude that it originates from the Raman scattering process. However, a large width of this band (213 cm^{-1}), which is essentially independent of the temperature, means that it is not attributable to fundamental modes.

We also studied Raman spectra of Na-deficient samples $Na_{1-x}V_2O_5$ ($x = 0$, 0.05, 0.10, 0.15). The most prominent changes occur in the A_g (aa) spectrum (see Fig. 7). The 447-cm^{-1} Raman line moves to higher frequencies as x increases. Its position shown by the vertical dashed

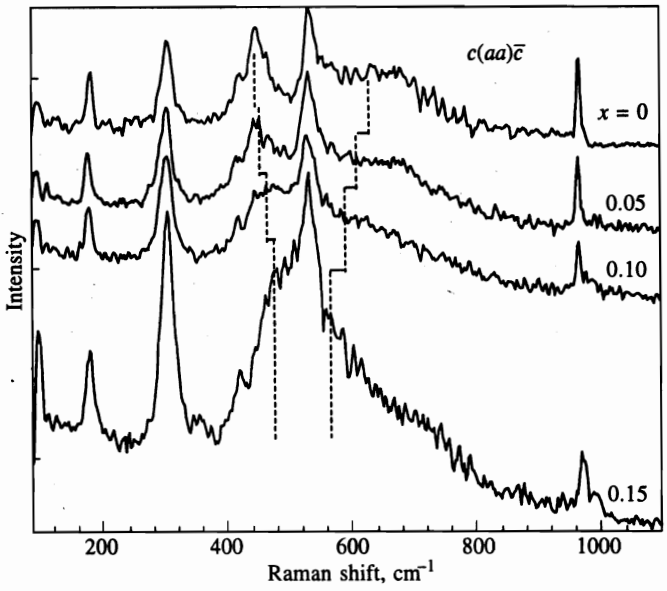

Fig. 7. Room-temperature Raman spectra of $Na_{1-x}V_2O_5$ for various x

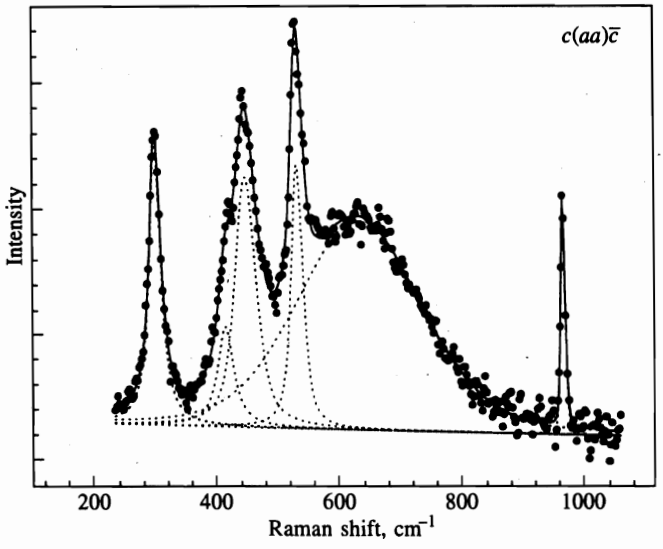

Fig. 8. Expansion of the room temperature $c(aa)\bar{c}$ Raman spectrum of NaV_2O_5 into individual profiles (dashed lines). The sum of these profiles, shown by a solid line, approximates the experimental spectrum (circles) well

lines in Fig. 7 is 477 cm^{-1} for the sample with $x = 0.15$. The maximum of the broad ba moves in the opposite direction, namely, from 632 cm^{-1} for $x = 0$ to 562 cm^{-1} for $x =$ This change of the frequency difference between these two Raman bands is, probably, due to a change in intermode interaction. The shape of the broad band can be approximated well by a Gaussian for all the values of x, its width growing from 213 cm^{-1} at $x = 0$ to 290 cm^{-1} at $x = 0.15$. As for phonon Raman lines, their shape is almost Lorenzian, and their width grows too. For example, the lines at 177, 301 and 531 cm^{-1} broaden from 11, 18 and 20 cm^{-1} at $x = 0$ to 16, 27 and 34 cm^{-1} at $x = 0.15$. The broadening of Raman bands with increasing x is probably associated with an increase in lattice disorder.

It is difficult to compare absolute intensities of the spectra at different x. However, certain conclusions concerning relative spectral intensities can be drawn. The most prominent features are a rise in intensity of the 301 cm^{-1} line, and the amergence of a new line at 988 cm^{-1} at $x = 0.15$. All these results were obtained by expanding the observed spectrum into individual spectral profiles. An example of such expansion is shown in Fig. 8.

3.4. Calculations of vibrational spectra

To obtain an information about the phonon spectrum of NaV_2O_5 throughout the Brillouin zone, which is necessary for the analysis of the spin–phonon interaction effects, we have considered the lattice dynamics of this crystal in the framework of the rigid ion model. The goal of this study is to display the basic pairwise interionic interactions that determine the main features of the measured Raman and infrared transmittance and reflection spectra.

A theoretical analysis of the vibrational spectra has been carried out for both lattice structures proposed in the literature. We did not obtain any physically well-grounded set of parameters which might provide the stable C_{2v}^7 lattice structure. We therefore discuss in this section only vibrations of the centrosymmetric lattice with the D_{2h}^{13} space group.

From the large measured large TO–LO splittings of some normal modes at the center of the Brillouin zone (Γ point), it is clear that long-range Coulomb forces play a crucial role in formation of the vibrational spectrum of NaV_2O_5. The potential energy of the lattice was represented by a sum of Coulomb and non-Coulomb interactions. The Coulomb terms in the dynamical matrix were calculated exactly using the Ewald method. Non-Coulomb interactions in the form of the Born–Mayer potentials with the exponential dependence on the interionic distance r ($\varphi_{ij}(r) = C_{ij}\exp(-r/\rho_{ij})$) were introduced between V–O (five bonds per vanadium ion), Na–O (eight bonds per sodium ion) and O–O neighboring ions at interionic distances less than 0.325 nm. Because of the nonequivalence of the oxygen O1, O2 and O3 ions we have to introduce different potentials for different types of bonding. In the initial step we confined ourselves to just ten fitting parameters (instead of the 34 independent force constants for the V_2O_5 lattice in Ref. [22]) including ion charges Z(A) (a condition of lattice neutrality brings the relation $Z(\mathrm{Na}) + Z(\mathrm{O1}) + 2Z(\mathrm{V}) + 2Z(\mathrm{O2}) + 2Z(\mathrm{O3}) = 0$ about) and C_{ij}, ρ_{ij} constants for V–O, Na–O and O–O pairs of ions. Starting values of the parameters were taken from the lattice dynamics simulations of $TmVO_4$ [27], $LuPO_4$ [28] and $NaNO_3$ [29].

An orthogonal transformation of the atomic displacements to symmetrized and normalized linear combinations, namely,

$$u_\alpha(\Gamma_{1u}, \mathrm{A}) = \frac{1}{2}\left[u_{1\alpha}(\mathrm{A}) + u_{2\alpha}(\mathrm{A}) + u_{3\alpha}(\mathrm{A}) + u_{4\alpha}(\mathrm{A})\right],$$

$$u_\alpha(\Gamma_{1g}, \mathrm{A}) = \frac{1}{2}\left[-u_{1\alpha}(\mathrm{A}) - u_{2\alpha}(\mathrm{A}) + u_{3\alpha}(\mathrm{A}) + u_{4\alpha}(\mathrm{A})\right],$$

$$u_\alpha(\Gamma_{2u}, \mathrm{A}) = \frac{1}{2}\left[-u_{1\alpha}(\mathrm{A}) + u_{2\alpha}(\mathrm{A}) - u_{3\alpha}(\mathrm{A}) + u_{4\alpha}(\mathrm{A})\right],$$

$$u_\alpha(\Gamma_{2g}, \mathrm{A}) = \frac{1}{2}\left[u_{1\alpha}(\mathrm{A}) - u_{2\alpha}(\mathrm{A}) - u_{3\alpha}(\mathrm{A}) + u_{4\alpha}(\mathrm{A})\right],$$

$$u_\alpha(\Gamma_{1u}, \mathrm{B}) = \frac{1}{\sqrt{2}}\left[u_{1\alpha}(\mathrm{B}) + u_{2\alpha}(\mathrm{B})\right],$$

$$u_\alpha(\Gamma_{1g}, \mathrm{B}) = \frac{1}{\sqrt{2}}\left[-u_{1\alpha}(\mathrm{B}) + u_{2\alpha}(\mathrm{B})\right],$$

where A, denotes V, O2, or O3 ions, and B denotes Na or O1 ions, divides the dynamical matrix at the Γ-point into blocks corresponding to irreducible representations of the crystal factor-group. Here,

$$\Gamma_{1u} = B_{3u}, \quad \Gamma_{1g} = B_{2g}, \quad \Gamma_{2u} = B_{1u}, \quad \Gamma_{2g} = A_g \quad \text{for} \quad \alpha = x,$$

$$\Gamma_{1u} = B_{2u}, \quad \Gamma_{1g} = B_{3g}, \quad \Gamma_{2u} = A_u, \quad \Gamma_{2g} = B_{1g} \quad \text{for} \quad \alpha = y,$$

$$\Gamma_{1u} = B_{1u}, \quad \Gamma_{1g} = A_g, \quad \Gamma_{2u} = B_{3u}, \quad \Gamma_{2g} = B_{2g} \quad \text{for} \quad \alpha = z.$$

Comparing the calculated eigenvalues of the dynamical matrix with the measured frequencies of the lattice normal modes, we varied the parameters Z,C_{ij},ρ_{ij} step-by-step in a physically motivated direction (e.g., absolute values of Z were diminished to account for the observed maximum LO–TO splittings) with the aim of achieving a better agreement with the measured frequencies at the Brillouin zone center. Simultaneously, frequencies of normal modes at zone boundaries and with the wave vectors **k** close to the Γ point (acoustical modes) were controlled.

The rigid-ion model presents a very crude approximation to the charge distribution in covalent compounds, and the optimization of the model parameters was terminated when achieving real values for the lattice normal modes frequencies throughout the Brillouin zone. The final values of the effective ionic charges were $Z(\mathrm{V}) = 2.405$, $Z(\mathrm{Na}) = 0.83$, $Z(\mathrm{O1}) = -1.22$, $Z(\mathrm{O2}) = -1.23$, $Z(\mathrm{O3}) = -0.98$ (in units of the proton charge), which are close to corresponding effective charges for vanadium $Z(\mathrm{V}) = 3$ and oxygen $Z(\mathrm{O}) = -1.5$ in $TmVO_4$ [27], phosphorus $Z(\mathrm{P}) = 2.33$ and oxygen $Z(\mathrm{O}) = -1.19$ in $LuPO_4$ [28], and sodium $Z(\mathrm{Na}) = 0.87$ in $NaNO_3$ [29]. The apical oxygen ion O3, closest to the vanadium ion, has the lowest charge due to its having the strongest covalent binding.

The calculated frequencies of the lattice normal modes at the Brillouin zone center are presented in Tables 1 and 2 for infrared and Raman active modes. The calculated frequencies of silent A_u modes are 120, 167 and 572 cm^{-1}. The acoustic properties of the lattice are defined by nine elastic constants, the predicted values of $C_{11} = 17.7$, $C_{12} = 9.7$, $C_{22} = 23.6$ (in units of 10^{10} $\mathrm{N/m^2}$) are less dependent on variations of the model parameters.

The measured components of the high-frequency dielectric tensor ε_∞ differ appreciably from unity (see Table 1), so neglect of electronic polarization is a very crude approximation in this case — in particular, when estimating LO–TO splittings at the Γ point. However, for most of the infrared active normal modes, our model yields a satisfactory description of the

longitudinal macroscopic electric field induced by the vibrations of ions. Very strong damping of the B_{1u} TO mode at 591 cm^{-1} may be the reason for the large difference between the calculated and measured LO–TO splitting (see Table 1); in the case of the B_{2u} TO mode at 365 cm^{-1}, our model yields a greatly overestimated frequency of the corresponding LO mode. Large discrepancies between several calculated frequencies of the Raman active modes and the experimental data (see Table 2) clearly demonstrate that some significant interactions — in particular, three-body forces, which strongly affect the frequencies of bending vibrations — are to be included in more thorough study of the lattice dynamics of this system.

Perhaps, the most interesting result of this analysis of the NaV_2O_5 lattice dynamics is the predicted soft mode behavior of the transverse acoustic mode at the Brillouin zone boundary (with the wave vector $\mathbf{k}_0 = \pi(0, 0, 1/c)$), polarized in the ac-plane. Due to the competition between long-range Coulomb and short-range non-Coulomb forces, the corresponding branch of the vibrational spectrum moves to the range of imaginary frequencies when approaching the $\mathbf{k}_0$ point thus making it possible to consider the NaV_2O_5 crystal an improper virtual ferroelastic. To stabilize the lattice against $\mathbf{k}_0$-excitations, we had to introduce an attractive interaction between neighboring V_1 and V_2 (V_3 and V_4) ions along the a-axis with the significant bending force constant of approximately 5 N/m. Charge ordering in the subsystem of V ions can destroy the balance between forces of opposite sign and induce freezing of the soft-mode atomic displacements (the unit cell doubles in the c direction, the neighboring layers shift in opposite directions, and in each layer the right and left legs of the vanadium ladders become nonequivalent, due to shifts of V_1–V_2 and V_3–V_4 rungs along opposite directions in the ac-plane) as a precursor of the subsequent magnetic ordering with doubling of a unit cell in a-, b- and c-directions.

4. DISCUSSION

4.1. Symmetry group of NaV_2O_5

Table 3 summarizes the observed vibrational modes together with their interpretation both in centrosymmetric D_{2h}^{13} and noncentrosymmetric C_{2v}^{7} groups. While the former group explains naturally the experimental data provided one Raman and three infrared frequencies remain undetected, the latter group leads to an assumption that 22 of 45 expected Raman and 23 of 37 expected infrared modes were not detected. Moreover, only three frequencies (90, 174, and 951 cm^{-1}) coincide to within the experimental accuracy (± 4 cm^{-1}) in the sets of Raman and infrared modes corresponding to a given irreducible representation of the noncentrosymmetric group, whereas all the modes should be both Raman and infrared active in that case. We also note once more that we failed to obtain a realistic set of force constants when carrying out the lattice dynamics calculations in the assumption C_{2v}^{7} noncentrosymmetric space group.

We consider our Raman and infrared data, and the results of lattice dynamics calculations, to support strongly the conclusion of the previous structural studies [13, 14] that the space group of NaV_2O_5 above $T_c = 35$ K is the centrosymmetric D_{2h}^{13} rather than noncentrosymmetric C_{2v}^{7} group. From the point of view of D_{2h}^{13} group it is also easy to explain the results of a recent ^{51}V-NMR study [16] that revealed only one vanadium position at elevated temperatures.

Table 3

Comparison of experimentally observed Raman and infrared modes with the expected ones within centrosymmetric D_{2h}^{13} and noncentrosymmetric C_{2v}^{7} space groups (mode frequencies are in cm^{-1})

$Pmmn(D_{2h}^{13})$	Observed modes	$Pmn2_1(C_{2v}^{7})$
$8A_g(aa, bb, cc)$	90 177 233 301 420 447 533 970	$15A_1(aa, bb, cc; \mathbf{E}\|\|\mathbf{a})$
$7B_{3u}(\mathbf{E}\|\|\mathbf{a})$	91[a] 145 251 526 939	
$3B_{1g}(ab)$	174 295 683	$7B_1\ (ab; \mathbf{E}\|\|\mathbf{b})$
$4B_{2u}(\mathbf{E}\|\|\mathbf{b})$	175 225[a] 367 582	
$8B_{2g}(ac)$	141 186 225 392 429 550 951	$15B_2\ (ac; \mathbf{E}\|\|\mathbf{c})$
$7B_{1u}(\mathbf{E}\|\|\mathbf{c})$	162 179 468 591 760 955	
$5B_{3g}(bc)$	169 257 366 418 683	$8A_2\ (bc)$
$3A_u$		

[a] Observed below 200 K.

4.2. Atomic displacements

As we have mentioned in the Introduction, the structure of NaV_2O_5 looks like the structure of V_2O_5 intercalated with Na. The V–O bond lengths within the vanadium-oxygen layers are close in these two compounds (see Table 4). The longest bond within the layer interconnects two V_2O_5 units in the crystal unit cell (see Fig. 1b where this bond is indicated by a dashed line). Thus, it makes a certain amount of sense to classify the $k = 0$ crystal vibrations on the basis of internal vibrations of the V_2O_5 «molecule» (C_{2v} point symmetry group), split into Davydov doublets of the D_{2h} factor group by an interaction between two «molecules» in the crystal unit cell. $(A_g + B_{1u})$, $(B_{2g} + B_{3u})$, $(B_{3g} + B_{2u})$, and $(B_{1g} + A_u)$ Davydov doublets come, respectively, from A_1, B_1, B_2, and A_2 vibrations of the V_2O_5 «molecule». Splittings of these doublets can be as great as 100 cm^{-1} due to Coulomb interactions and, in particular, due to interactions between adjacent V ions via common neighbors (O2 ions) along the chains (see Fig. 1). Many of the vibrational frequencies of Na V_2O_5 are close to those of V_2O_5 [22].

A comparison of our observed vibrational frequencies with those of V_2O_5 [22] and with the results of our calculations leads to the following assignment of the vibrational modes of NaV_2O_5. The V–O3 stretching modes are manifested by two Davydov doublets: 951 cm^{-1} (B_{2g}) + 939 cm^{-1} (B_{3u}) and 970 cm^{-1} (A_g) + 955 cm^{-1} (B_{1u}). The Davydov splittings are relatively small in this case, indicating that these vibrations associated with the strongest bond V–O3 are really well localized. The mode frequencies are somewhat lower than the corresponding frequencies in V_2O_5 (976, 982, 994, and 975 cm^{-1}), which is consistent with longer V–O3 bonds in NaV_2O_5 in comparison with V_2O_5. The following vibrations are associated with the O1–V–O3 bending modes: 177 cm^{-1} (A_g), 162 cm^{-1} (B_{1u}), 392 cm^{-1} (B_{2g}), 366 cm^{-1} (B_{3g}).

Table 4

The bond lengths (nm) in NaV_2O_5 and V_2O_5

Bond	NaV_2O_5 Ref. [13]	V_2O_5 Ref. [22]
V–O3	0.161	0.158
V–O1	0.183	0.177
(V–O2)×2	0.192	0.188
V–O2′	0.199	0.202
V–O3′	0.318	0.278

The bridging oxygens O1 participate in V–O1–V bending vibrations 418 cm^{-1} (B_{3g}), 367 cm^{-1} (B_{2u}), 447 cm^{-1} (A_g), and 468 cm^{-1} (B_{1u}). The V–O1–V stretching vibration is located at 420 cm^{-1} (A_g) and mainly involves the motion of the V atoms along the a-axis.

The modes at 683 cm^{-1} (B_{3g} and B_{1g}) and 582 cm^{-1} (B_{2u}) correspond to V–O2 stretching vibrations along the b-axis, while those at 550 cm^{-1} (B_{2g}), 533 cm^{-1} (A_g), and 526 cm^{-1} (B_{3u}) correspond to the bending vibrations.

Most of the remaining modes can be described in terms of external modes of the V_2O_5 units. Thus, the modes at 186 cm^{-1} (B_{2g}), 169 cm^{-1} (B_{3g}) and 90 cm^{-1} (A_g), correspond to the relative translations of the two V_2O_5 units within the crystal unit cell along the a-, b-, and c-axes, respectively. As the V_2O_5 units are bind along the b-axis, these modes can be considered relative translations of neighboring $(VO_5)_n$ chains. The B_{1g} mode at 174 cm^{-1} (O3 ions move along the b-axis) and the A_g mode at 301 cm^{-1} (O2 ions move along the c-axis) correlate with in-plane and out-of-plane chain bending vibrations, respectively. The B_{2g} mode at 141 cm^{-1} and B_{3u} mode at 91 cm^{-1} are associated with rotation of the chains around the b-axis.

Modes that involve mainly displacements of Na atoms are at 225 cm^{-1} (B_{2u}), 251 cm^{-1} (B_{3u}), and 179 cm^{-1} (B_{1u}).

4.3. Spectra of electron excitations

With our derived values of the effective charges, we estimated the crystal field energies of the 3d electron localized at a V^{4+} ion site. The crystal field parameters $B_2^0 = 1360 + 2090G$, $B_2^1 = 2020 - 1590G$, $B_2^2 = 820 + 640G$, $B_4^0 = 610 + 1430G$, $B_4^1 = -1810 - 3690G$, $B_4^2 = 33 + 144G$, $B_4^3 = 3650 + 8180G$, $B_4^4 = 4070 + 7420G$ cm^{-1} for the V_1 and V_3 sites were calculated in the framework of the exchange charge model [30] (for the V_2 and V_4 sites B_p^1 and B_p^3 parameters change signs; the first terms correspond to point charge contributions, and Stevens normalization is used). The scaling factor G determines the strength of the exchange charge field. We estimated this phenomenological parameter of the model ($G = 4$) by fitting the total crystal field splitting to the width of the V-3d bands presented in Ref. [13]. In this case, the effective crystal field provides the following energy level pattern of the V^{4+} ion : 0 (A''), 1.10 (A'), 1.18 (A''), 3.39 (A') and 4.78 (A') eV (irreducible representations of the C_s point group, corresponding to the space symmetry of the electron wave function, are given in brackets, additional shifts of the crystal field levels due to the spin-orbit interaction and the electrostatic field of a hole at the neighboring vanadium site are less than 0.025 eV). The ground state wave function is the d_{xy} orbital with small admixture of the d_{yz} orbital, as prevoiusly pointed out, [13] and the sequence of the excited states is in agreement with band structure calculations as

well [13].

Strong absorption of light (**k**||**c**) with **E**||**a** as well as with **E**||**b** was observed in the region 1.0–1.2 eV [21]. Both magnetic dipole and induced electric dipole d–d transitions in the odd crystal field are allowed between the A″ states for **E**||**a**, and between the A″ and A′ states for **E**||**b**. Thus, in accordance with the results on crystal field energies given above, the observed broad optical bands in the vicinity of 1 eV can be interpreted as phonon assisted d–d transitions without any additional suppositions about the broken symmetry between the legs of vanadium ladders [31].

The next step towards the detailed description of the spectra of electron excitations is to construct molecular orbitals for the $[V_2O]^{7+}$ «molecule», which has C_{2v} point symmetry, using vanadium d-orbitals and oxygen p-orbitals. The vanadium ground state wave function d_{xy} yields the nonbonding a_2 orbital as well as bonding B_2 and antibonding b_2^* molecular orbitals, namely,

$$a_2 : \left[d_{xy}(\mathrm{L}) + d_{xy}(\mathrm{R})\right], \quad b_2 : \left[d_{xy}(\mathrm{L}) - d_{xy}(\mathrm{R})\right] + p_y, \quad b_2^* : \left[d_{xy}(\mathrm{L}) - d_{xy}(\mathrm{R})\right] - p_y.$$

Here, a_2, b_2 denote irreducible representations of the C_{2v} point group and L and R denote vanadium sites on the left and right sides of a ladder rung. The highest filled orbital being a_2, the $a_2 \to b_2^*$ electronic transition allowed in **E**||**a** polarization can account for the low-frequency absorption band observed only in this polarization. Quantum-chemical calculations are necessary to verify this qualitative interpretation.

4.4. Fano resonances with a continuum

The asymmetric line shapes of the infrared active modes at 91, 150, 939 cm^{-1} in **E**||**a** polarization highlight the strong interference between these modes and a continuum, observed just in this polarization. This interpretation is supported by the fact that the spectral line near 91 cm^{-1} becomes perfectly symmetric when the continuum absorption vanishes in this spectral range below the phase transition temperature $T_c = 35$ K. In our earlier work [8] we argued that these changes are related to the opening of a gap in the magnetic excitation spectrum at T_c, the observed continuum being due to two-magnon absorption.

However, such a straightforward interpretation is no longer valid in the case of the space group D_{2h}^{13}. It must be revised, taking into account possible electronic excitations in this frequency range, as discussed in the previous section, and charge ordering at the transition temperature.

4.5. Higher order infrared vibrational spectra

Two- and three-phonon absorption results from anharmonicity of crystal vibrations. It is continuous, displaying singularities corresponding to critical points of the Brillouin zone. Leaving the detailed analysis of multiphonon bands to the future, we discuss here only sharp lines observed in **E**||**c** absorbance spectrum (Fig. 5). They are listed in Table 5 together with their tentative assignment, using symmetry-allowed combinations of Γ-point phonons observed in our first-order spectra. The coincidence of the observed and combinational frequencies lies within the accuracy of our measurements.

The strongest narrow peak at 1930 cm^{-1} corresponds, according to this assignment, to sum of the components of the Davydov doublet originating from the V–O3 stretching vibration. This stretching mode is well localized, which results in its small dispersion over the Brillouin zone, thus delivering a narrow two-phonon band, in accordance with the experimental observation.

Table 5

Multiphonon bands in NaV_2O_5 observed in E||c polarization

Observed bands, cm^{-1}	Combination of phonons, cm^{-1}
1072 (B_{1u})	550 (B_{2g}) + 526(B_{3u}) = 1076(B_{1u})
1270 (B_{1u})	683 (B_{3g}) + 582(B_{2u}) = 1265(B_{1u})
1930 (B_{1u})	970 (A_g) + 955(B_{1u}) = 1925(B_{1u})
2858 (B_{1u})	3 × 955(B_{1u}) = 2865(B_{1u})
2901 (B_{1u})	2 × 970(A_g) + 955(B_{1u}) = 2895(B_{1u})

5. SUMMARY

We have performed a thorough spectroscopic study of far infrared reflectance and transmittance, along with Raman scattering of α'-NaV_2O_5 single crystals in the high-temperature phase (above T_c = 35 K). Far infrared spectra were obtained for **E||a**, **E||b**, and **E||c** polarizations of incident light. Diagonal (*aa*), (*bb*), (*cc*) and off-diagonal (*ab*), (*bc*), (*ac*) components of the Raman scattering tensor were investigated. We report five infrared active modes in **E||a** polarization, four in **E||b** polarization, and six in **E||c** polarization. Eight Raman active modes have been detected for parallel polarizations of incident and scattered light (*aa*), (*bb*), (*cc*). The (*ab*), (*ac*) and (*bc*) Raman geometries delivered three, seven, and five modes, respectively. These results are in much better agreement with the recently proposed centrosymmetric space group D_{2h}^{13} ($Pmmn$) for the high-temperature phase of NaV_2O_5 than with the previously adopted noncentrosymmetric space group C_{2v}^7 ($Pmn2_1$). We have also carried out the lattice dynamics calculations, based on the rigid ion model for both structures of NaV_2O_5 proposed in the literature. We failed to obtain any physically well-grounded set of parameters providing a stable C_{2v}^7 lattice structure. Thus, our infrared and Raman experimental data, along with the results of lattice dynamics calculations, strongly support the conclusion of the previous structural study [13, 14] that the space group of NaV_2O_5 above T_c = 35 K is the centrosymmetric D_{2h}^{13} rather than noncentrosymmetric C_{2v}^7 group.

This conclusion leads to important physical consequences. In particular, it requires a revisd interpretation of one-dimensional magnetic properties of NaV_2O_5 and of the phase transition at 35 K, previously considered as an ordinary spin-Peierls transition. The interpretation of the previously observed broad bands in near and far infrared absorption [8, 21] needs to be reconsidered as well.

Using the effective charges derived via lattice dynamics calculations, and fitting the total crystal field splitting to the width of the V–3*d* bands [12], we estimated the crystal field energies of the 3*d* electron localized at the vanadium site. It follows from this estimate that the observed [21] near infrared broad band absorption of NaV_2O_5 can be interpreted as phonon-assisted *d*–*d* transitions. We speculate that the far infrared **E||a** polarized absorption continuum might be associated with electron excitations of $[V_2O]^{7+}$ rungs in a crystal field of C_{2v} symmetry.

Strongly asymmetric spectral lines observed in **E||a** absorbance spectra of NaV_2O_5 highlight a strong interference between relatively narrow phonon lines and the underlying continuum. This suggest an interaction between crystal vibrations and magnetic or electronic excitations. The detailed physical interpretation of the observed phenomenon depends on the nature of the

far infrared E||a polarized continuum, which requires special investigation.

In conclusion, we reported also some preliminary results on higher-order vibrational spectra of NaV_2O_5 resulting from anharmonicity of lattice vibrations.

After having submitted this paper for publication (see [32]) we became aware of a similar investigation [33, 34]. Experimental data presented in these papers are in good agreement with our results.

We are grateful to A. I. Smirnov for checking the samples by ESR measurements, to A. N. Vasil'ev for stimulating discussions, and to G. N. Zhizhin for sustained support of this research. This work was made possible in part by Grant No. 98-02-17620 from the Russian Foundation for Basic Research.

References

1. M. Isobe and Y. Ueda, J. Phys. Soc. Jap. **65**, 1178 (1996).
2. A. I. Buzdin and L. N. Bulaevskii, Usp. Fiz. Nauk **131**, 495 (1980) [Sov. Phys. Usp. **23**, 409 (1980)].
3. J. Hemberger, M. Lohmann, N. Nickloas, A. Loidl, M. Klemm, G. Obermeier, and S. Horn, Europhys. Lett. **42**, 661 (1998); T. Yamada, private communication.
4. K. Kobayashi, T. Mizokawa, A. Fujimori, M. Isobe, and Y. Ueda, Phys. Rev. Lett. **80**, 3121 (1998).
5. Y. Fujii, H. Nakao, T. Yoshihama, M. Nishi, K. Nakajima, K. Kakurai, M. Isobe, Y. Ueda, and H. Sawa, J. Phys. Soc. Jap. **66**, 326 (1997).
6. M. Weiden, R. Hauptmann, C. Geibel, F. Steglich, M. Fisher, P. Lemmens, and G. Guntherodt, Z. Phys. B **103**, 1 (1997).
7. H. Curoe, H. Seto, J. Sasaki, T. Sekine, M. Isobe, and Y. Ueda, submitted to J. Phys. Soc. Jap.; E-prints archive cond-mat/9805251.
8. M. N. Popova, A. B. Sushkov, A. N. Vasil'ev, M. Isobe, and Y. Ueda, Pis'ma Zh. Èksp. Teor. Fiz. **65**, 711 (1997) [JETP Lett. **65** 743 (1997)]; E-prints archive cond-mat/9711052.
9. D. Smirnov, P. Millet, J. Leotin, D. Poilblanc, J. Riera, D. Augier, and P. Hansen, Phys. Rev. B **57**, R11035 (1998).
10. T. Yoshihama, M. Nishi, K. Nakajima, Y. Fujii, M. Isobe, and Y. Ueda, Physica B **234–236**, 539 (1997).
11. A. Carpy and J. Galy, Acta Crystallogr. B **31**, 1481 (1975).
12. H. G. Backman, F. R. Ahmed, and W. H. Barnes, Z. Krist. **115**, 110 (1961).
13. H. Smolinski, C. Gros, W. Weber, U. Peuchert, G. Roth, M. Weiden, and C. Geibel, Phys. Rev. Lett. **80**, 5164 (1998).
14. A. Meetsma, J.L. de Boer, A. Damascelli, T. T. M. Palstra, J. Jegoudez, and A. Revcolevschi, Acta Cryst. C **54**, 1558 (1998).
15. P. Horsch and F. Mack, E-prints archive cond-mat/9801316.
16. T. Ohama, H. Yasuoka, M. Isobe, and Y. Ueda, Phys. Rev. B **59**, 3299 (1999).
17. H. Seo and H. Fukuyama, E-prints archive cond-mat/9805185.
18. M. V. Mostovoy and D. I. Khomskii, E-prints archive cond-mat/9806215.
19. P. Thalmeier and P. Fulde, E-prints archive cond-mat/9805230.
20. M. Köppen, D. Pankert, R. Hauptmann, M. Lang, M. Weiden, C. Geibel, and F. Steglich, Phys. Rev. B **57**, 8466 (1998).
21. S. A. Golubchik, M. Isobe, A. N. Ivlev, B. N. Mavrin, M. N. Popova, A. B. Sushkov, Y. Ueda, and A. N. Vasil'ev, J. Phys. Soc. Jap. **66**, 4042 (1997).
22. L. Abello, E. Husson, Y. Repelin, and G. Lucazeau, Spectrochem. Acta **39A**, 641 (1983).
23. M. Isobe, C. Kagami, and Y. Ueda, J. Crystal Growth **181**, 314 (1997).

24. B. N. Mavrin, Optika i Spectroscopiya **49**, 79 (1980).
25. D. L. Rousseau, R. P. Bauman, and S. P. S. Porto, J. Raman Spectr. **10**, 253 (1981).
26. U. Fano, Phys. Rev. **124**, 1866 (1961).
27. V. R. Pekurovskii, Izvestiya AN USSR, Ser. Fiz. **50**, 324 (1986).
28. J. C. Nipko, C.-K. Loong, M. Loewenhaupt, M. Braden, W. Reichardt, and L. A. Boatner, Phys. Rev. B **56**, 11584 (1997).
29. A. Yamamoto, T. Utida, H. Murata, and Y. Shiro, J. Phys. Chem. Sol. **37**, 693 (1976).
30. B. Z. Malkin, in *Spectroscopy of solids containing rare-earth ions*, ed. by A. A. Kaplyanskii and R. M. Macfarlane, Elsevier Science PB, Amsterdam (1987), pp. 13–49.
31. A. Damascelli, D. van der Marel, J. Jegoudez, G. Dhalenne, and A. Revcolevschi, E-prints archive cond-mat/9806222.
32. M. N. Popova, A. B. Sushkov, S. A. Golubchik, B. N. Mavrin, V. N. Denisov, B. Z. Malkin, A. I. Iskhakova, M. Isobe, and Y. Ueda, E-prints archive cond-mat/9807369.
33. Z. V. Popović, M. J. Konstantinović, R. Gajić, V. Popov, Y. S. Raptis, A. N. Vasil'ev, M. Isobe, and Y. Ueda, J. Phys.: Cond. Matt. **10**, L513 (1998).
34. D. Smirnov, J. Leotin, P. Millet, J. Jegoudez, and A. Revcolevschi, E-prints archive cond-mat/9808006.